# Dipolarization fronts and associated auroral activities: 1. Conjugate observations and perspectives from global MHD simulations

Y. S. Ge,[1] X.-Z. Zhou,[2] J. Liang,[3] J. Raeder,[1] M. L. Gilson,[1] E. Donovan,[3] V. Angelopoulos,[2] and A. Runov[2]

Received 1 March 2012; revised 27 August 2012; accepted 30 August 2012; published 25 October 2012.

[1] Earthward-propagating dipolarization fronts (DFs) are often found to be associated with magnetic reconnection and bursty bulk flows (BBFs) in the magnetotail. Recent THEMIS (Time History of Events and Macroscale Interactions During Substorms) probe observations have shown a DF propagating over 10 $R_E$ from the mid-tail region to the near-Earth tail region, and THEMIS All-Sky Imager data show a north-south auroral form and intensification of westward auroral zone currents. In this study, we examine THEMIS in situ observations of DFs in the magnetotail and simultaneous observations of the proton aurora from ground-based CANOPUS (the Canadian Auroral Network for the OPEN Program Unified Study) Meridian Scanning Photometers (MSPs). We find that earthward-moving DFs are often associated with intensification of proton aurora when the THEMIS probes are conjugate to the meridian of the MSP. The proton auroral intensifications are transient and in some cases detached from the background proton precipitation. Just before the DFs, the ion distribution is anisotropic in the field-aligned direction (mostly earthward) and the ion energy increases. These observations suggest that plasma sheet protons can be reflected and energized by earthward-moving DFs as they propagate through the magnetotail. We postulate that this population of ions is the source of the proton auroral intensification observed on the ground. This conjecture is tested using our global MHD simulation results, where the proton precipitation is calculated with the field-line curvature (FLC) model. The MHD simulation results show that proton precipitation enhancement can be caused by compression of plasma by approaching DFs/BBFs, which is consistent with ion reflection at DFs. Thus, using the conjugate observations from THEMIS spacecraft and MSP in this study, we are able to directly link the magnetotail dynamics, i.e., dipolarization fronts, with ground auroral activities. However, understanding of DF-associated ion energization requires detailed test-particle simulations with an analytical magnetotail model, such as those in our companion paper.

**Citation:** Ge, Y. S., X.-Z. Zhou, J. Liang, J. Raeder, M. L. Gilson, E. Donovan, V. Angelopoulos, and A. Runov (2012), Dipolarization fronts and associated auroral activities: 1. Conjugate observations and perspectives from global MHD simulations, *J. Geophys. Res.*, *117*, A10226, doi:10.1029/2012JA017676.

## 1. Introduction

[2] Bursty bulk flows (BBFs), transient, high-speed plasma flows responsible for significant flux transport in the magnetotail [*Angelopoulos et al.*, 1992, 1994], are important, dynamic magnetospheric events. Earthward BBFs are observed within a wide range of geocentric distances in the plasma sheet, from 5 $R_E$ to 30 $R_E$. An essential feature of these BBFs, enhancement of their magnetic field's Bz component and a corresponding decrease in plasma pressure [*Ohtani et al.*, 2004], is often called "magnetic field dipolarization". The enhanced magnetic flux carried by BBFs also implies reduction in plasma tube entropy (described in the bubble model; see reviews in *Wolf et al.* [2009]). As this bubble propagates earthward, interaction of the plasma-depleted flux tube with the ambient plasma produces a thin boundary layer called a "dipolarization front" (DF). THEMIS multispacecraft measurements ave provided more detailed observations of DFs, which are characterized by a sharp jump in Bz associated with a density drop and often preceded by a Bz dip and

[1]Space Science Center, University of New Hampshire, Durham, New Hampshire, USA.
[2]Department of Earth and Space Sciences and Institute of Geophysics and Planetary Physics, University of California, Los Angeles, California, USA.
[3]Department of Physics and Astronomy, University of Calgary, Calgary, Alberta, Canada.

Corresponding author: Y. S. Ge, Space Science Center, University of New Hampshire, 8 College Rd., Morse Hall, Rm. 244, Durham, NH 03824, USA. (yasong.ge@gmail.com)


0148-0227/12/2012JA017676

transient density enhancements [e.g., *Nakamura et al.*, 2002; *Runov et al.*, 2009, 2011a].

[3] Recently many authors have investigated dipolarization front properties and generation mechanisms using THEMIS and Cluster observations [e.g., *Runov et al.*, 2009; *Hwang et al.*, 2011]. The BBF-type flux rope [*Slavin et al.*, 2003] and nightside flux transfer event (NFTE) [*Sergeev et al.*, 1992] models seek to explain transient DFs, and recent kinetic simulations suggest that DF signatures can be produced by impulsive magnetic reconnection [*Sitnov et al.*, 2009]. Dipolarization front propagation and evolution have been investigated within a large range of geocentric distances using global MHD simulations [*Ge et al.*, 2011] in which DFs formed in front of a strong earthward BBF associated with auroral intensifications during substorms. In observations and simulations, BBF onset has been found to precede DFs. According to *Zhou et al.* [2011], the so-called "precursor flows" upstream of DFs are caused by reflection and acceleration of ambient plasma by approaching DFs.

[4] Earthward penetration of BBFs often causes perturbations in the geomagnetic field and auroral activity as a system of field-aligned currents (FACs) is generated to link BBFs to the ionosphere [e.g., *Sergeev et al.*, 1996; *Birn et al.*, 2004; *Nakamura et al.*, 2004]. The magnetic shear caused by this penetration is equivalent to FACs at the edge of BBFs. Electrons accelerated by the potential drop in FACs can produce auroral brightening in the ionosphere, such as poleward boundary intensifications [e.g., *Zesta et al.*, 2000] or substorm intensifications [e.g., *Ge et al.*, 2011]. Precipitation of protons during these dynamic events has seldom been investigated, however, because coverage from multispectrum observations of auroral activity has been limited. Proton precipitation from the nightside magnetosphere is usually caused by pitch angle scattering of plasma sheet protons into the downward loss cone [*Donovan et al.*, 2003a]. Observations of proton precipitation are particularly useful for monitoring the configurations of the magnetotail field and the plasma sheet. For example, the location of the isotropy boundary (known as IB or b2i), corresponding to the low-latitude boundary of proton aurora, marks the boundary between the empty and full downward loss cones and the location where the ion gyroradius become comparable to a radius of the field line curvature. More importantly, these observations provide information on the configuration of the nightside magnetosphere field, i.e., how stretched the magnetotail is and where the transition region between tail-like and dipole-like field is located [*Sergeev and Gvozdevsky*, 1995; *Donovan et al.*, 2003b].

[5] In addition to providing a global picture of magnetotail status, proton precipitation auroral observation can be used to investigate plasma sheet dynamics despite the diffuse nature of proton aurora (*Galand and Chakrabarti* [2006], review). Proton auroral variations during substorms were first investigated by *Montbriand* [1971] and *Fukunishi* [1975] using meridian-scanning tilting-filter photometers. Subsequently, comparisons between locations of proton aurora and auroral onsets have been extensively examined by many authors. Using observations from the CANOPUS array of MSPs and the DMSP satellite, *Samson et al.* [1992] concluded that substorm onset originated within proton precipitation as suggested by substorm onset theories based on resonance effects on closed, dipolar field lines. This conclusion was not supported, however, by observations studied by *Deehr and Lummerzheim* [2001]. *Deehr and Lummerzheim* [2001] found that the auroral substorm originated poleward of the dipolar field lines from the separation and very different temporal behavior of the onset arc and the peak proton precipitation. IMAGE spacecraft observations of proton aurora were summarized by *Mende et al.* [2003], who found the proton aurora to be located equatorward of the electrons in duskward onset sectors, but poleward in dawnward onset sectors. By investigating 35 typical substorm breakup events, *Takahashi and Fukunishi* [2001] found that when electron auroral arcs were enhanced and moved poleward after onsets, the proton auroral region also expanded poleward and formed a sharp poleward boundary coinciding with the leading edge of the electron auroral bulge. They also found that the most energetic precipitating protons appeared near the poleward boundary of proton aurora rather than in the intensity peak and concluded that the N-S auroral region corresponded to the plasma injection region in the magnetosphere. *Gilson et al.* [2011] also reported dynamical proton auroral variations during substorms; in a subsequent paper [*Gilson et al.*, 2012], they interpreted proton aurora splitting after substorm onsets as caused by penetration of dipolarization regions.

[6] Simultaneous ground and low-altitude satellite observations have frequently been used to study proton precipitation [e.g., *Donovan et al.*, 2003a]. Investigations using simultaneous observations of proton auroral variations and their magnetospheric sources have rarely been done, however, because of limited coverage from ground MSPs and consequently the small number of events with magnetic-conjugate observations from both the ground and the magnetotail. Conjugation of multipoint measurements in the magnetotail from THEMIS in its tail seasons [*Angelopoulos et al.*, 2008] with those from an array of ground stations in the North America provides a good opportunity to perform such studies. In this paper, we investigate proton auroral variations in two DF events during THEMIS-observed substorms using CANOPUS MSP observations and conjugate magnetic field and particle measurements by THEMIS spacecraft in the plasma sheet. By connecting ionospheric proton precipitation with magnetotail dynamics such as dipolarization fronts, this study attempts to provide new insight into physical processes responsible for proton auroras. In addition, by elucidating DF-associated ion dynamics, we seek to better understand plasma sheet ion acceleration and re-distribution processes other than those from magnetic reconnection. In the second part of this paper we use global MHD simulations to investigate DF-associated proton precipitation and its magnetospheric sources. This investigation provides us with magnetohydrodynamic perspectives on the interaction of DFs with the ambient plasma sheet.

## 2. THEMIS Observations of Dipolarization Fronts

### 2.1. Dipolarization Fronts During the 27 February 2009 Substorm

[7] The first dipolarization front event was observed by all five THEMIS spacecraft (also referred to as probes P1 to P5) during the expansion phase of a strong substorm on 27 February 2009. Figures 1a and 1b show the orbits of those probes projected on the XZ and XY planes in Geocentric

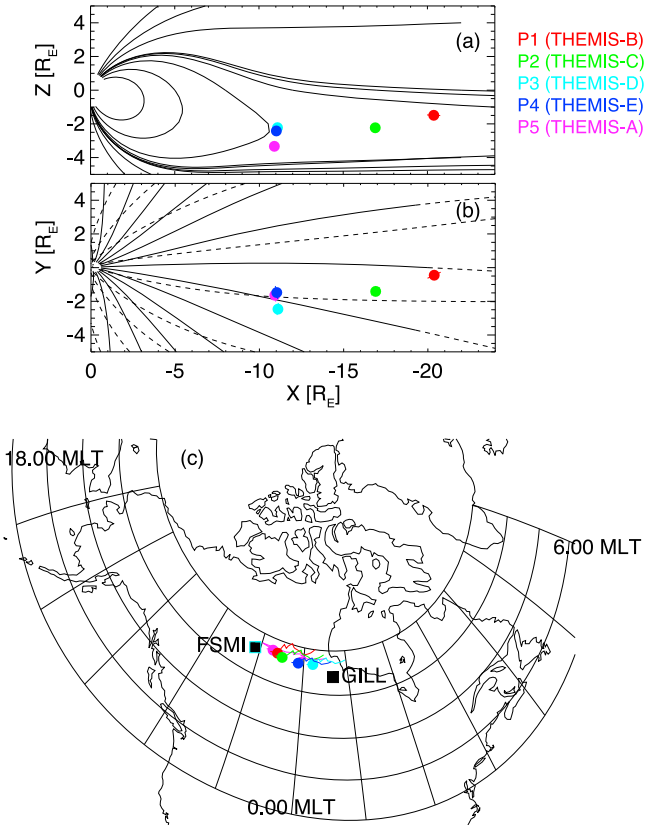


**Figure 1.** Projection of THEMIS probe orbits in the (a) XZ and (b) XY planes with T96 field lines on 27 February 2009; (c) THEMIS probe footprints from T96 model mapping.

Solar Magnetospheric (GSM) coordinates from 07:00 to 08:00 UT. The magnetic field lines in this figure are produced by the Tsyganenko 96 (T96) model. In the second tail season of the THEMIS mission, from December 2008 to April 2009, the inclination angles of the mid-tail probe (P1 and P2) orbits were reduced so that the two could better observe the thin current sheet in the magnetotail. In Figures 1a and 1b, we find that the five THEMIS probes were radially aligned. The outermost, P1, was located at ~21 $R_E$ downtail near the local midnight sector; P2 was at 17 $R_E$; and the three inner spacecraft (P3, P4, and P5) were near 11 $R_E$ downtail. It is noteworthy that of the three inner spacecraft, P5 is farthest from the central plasma sheet (CPS), which is consistent with the dominant Bx component at its location (not shown). The footprints of five THEMIS probes traced from the T96 model are shown in Figure 1c; the symbols mark the probes conjugate positions at 07:50 UT. We can see from this panel that the five probes map into the local time sectors between Fort Smith (FSMI) and Gillam (GILL) and that THEMIS P1, P2, and P5 are closer to FSMI than the other probes.

[8] Figure 2 shows observations at the five THEMIS probes, including the Bz component of the observed magnetic field and the x component of the plasma velocity, both in GSM coordinates, from the top to bottom panels (P1 to P5). At 07:50:25 UT, P1 observed a sharp dipolarization front, i.e., a sudden Bz component increase, following a transient Bz component decrease. Here we mark the DF arrival time at the minimum of the Bz component just prior to the sharp dipolarizations. *Runov et al.* [2009] investigated these dipolarization fronts in detail and interpreted the observations as the leading edge of a plasma fast flow formed by a burst of magnetic reconnection in the mid-tail, which is also shown in the kinetic simulation of impulsive reconnections by *Sitnov et al.* [2009]. All dipolarization fronts observed by the five probes were accompanied by fast earthward flows; the front structures were slightly different at each probe. The DF precursor, i.e., negative Bz before the sharp DF, was most pronounced at P4 and less so at P1. The Bz component remained positive at the other probes, even though it had a brief dip before the DF. This difference was attributed to the limited BBF size and the curved shape of the horizontal cross-section of the plasma-depleted flux tube. In this event, the normals of dipolarization fronts at THEMIS spacecraft has been derived by *Runov et al.* [2009] using the Minimum Variance Analysis (MVA). They have shown that in the XZ plane the normal of the DF points northward. Given that P4 is located southward of P3, P4 is closest to the thin interface of DF. At this interface, an intense vertical current sheet forms due to the interaction of the Earthward BBF and the plasma sheet. It has been shown by *Sergeev et al.* [2009] that the intensity of this current can be 10 times larger than the horizontal cross-tail current, which produces the large Bz variations across the DF. It appears that P4, in this event, is closest to the thin current sheet and observes the strongest Bz decrease ahead of the DF. By assuming that the observed DF propagates from P1, P2 to the inner THEMIS spacecraft, the propagation speed of the DF from 20 $R_E$ to 11 $R_E$ was estimated to be 300 km/s by *Runov et al.* [2009] from timing between P1, P2 and the inner spacecraft. Through in situ velocity measurements the front thickness of the DF was estimated to be about 400–500 km [*Runov et al.*, 2009]. However, the assumption that the DF at P1 and P2 is the same as that observed by P3, P4, and P5 is questioned by later studies. Using THEMIS ASI observations, *Lyons et al.* [2012] suggested that the DF observed by P3, P4, and P5 was different from that observed by P1 and P2. In the ASI observations, these two fronts were found to produce two separate streamers. In this study, the DFs observed at the middle tail by P1 and P2 are also considered to be different events from those observed by P3, P4 and P5.

[9] Figure 3 gives the azimuthal angle distributions of protons around DFs observed by THEMIS probes. Figure 3a shows the observed Bz components of the magnetic field at five probes for reference. Figures 3b–3f show the observed differential flux of 5–25 keV ions versus azimuthal angle. The vertical lines on Figures 3b–3g mark DF arrival times at each probe, and the spectrum after the DF arrivals has been shaded. The arrival times of DFs here are marked by the minimum of the Bz components that is immediately prior to the sharp enhancement of the Bz component in the dipolarization region. For example, the DF arrival times at P1, P2, P3 and P4 are marked at 07:51:26, 07:52:35, 07:54:06 and 07:54:10 UT respectively. However, at P5, the buildup of Bz is more gradual than those at other spacecraft. We mark 07:53:34 UT as the arrival time of DF at P5, when the Bz component reaches a minimum prior to the following dipolarization. Thirty seconds to one minute prior to DF arrival, the azimuthal angles of ions at all five probes are distributed around 0°, which corresponds to the earthward direction. This type of ion distribution is often seen in the precursor flow upstream of dipolarization fronts. Consisting of the new

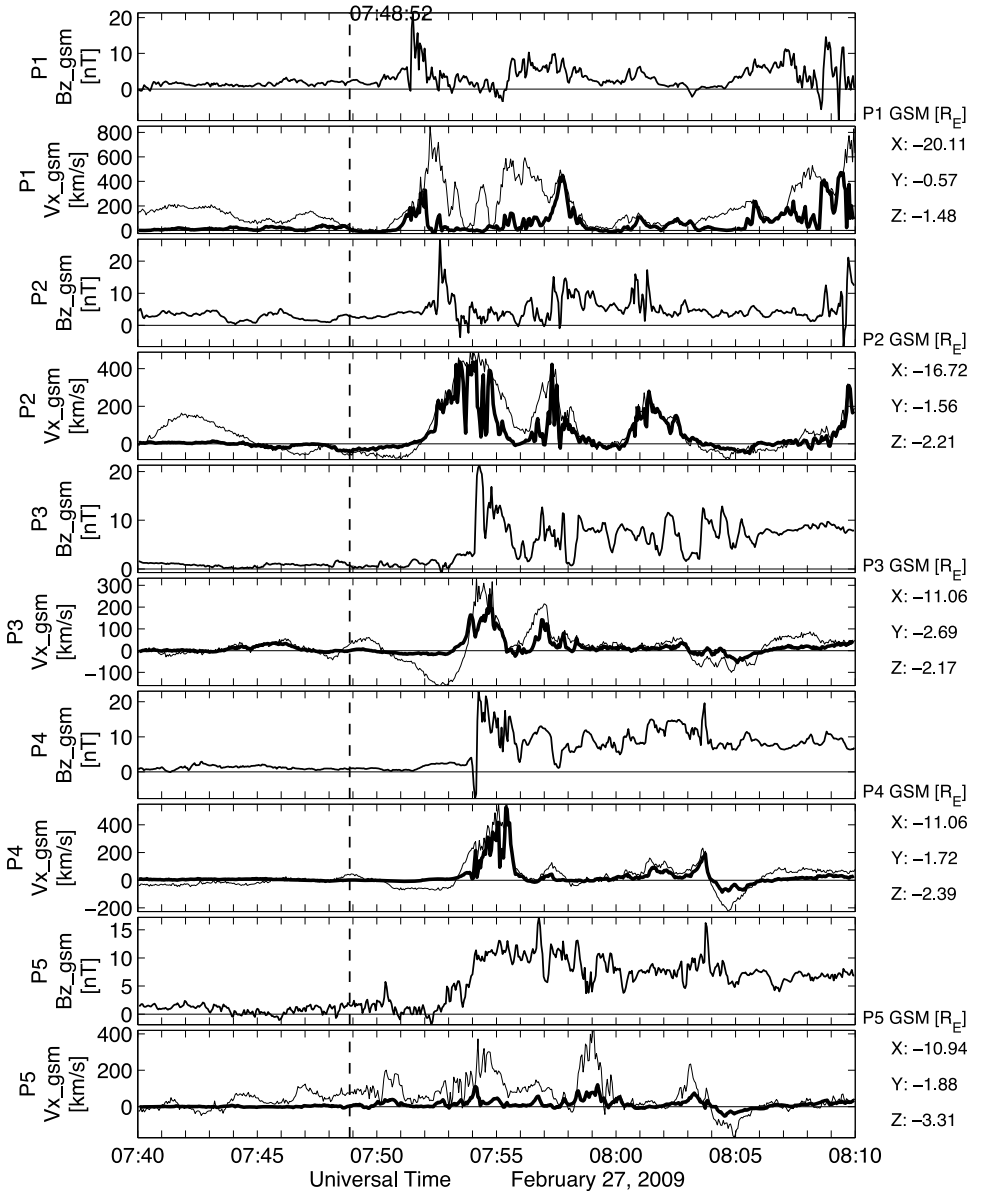


**Figure 2.** Bz and plasma velocity Vx components in GSM coordinates observed by five THEMIS probes on 27 February 2009. The thin lines represent THEMIS ESA plasma velocity measurements in the GSM x direction; the thick lines are the x-component of the velocity perpendicular to the local magnetic field orientation. The vertical line marks the substorm's AE onset time; the locations of five probes at AE onset are shown at the right of the panels.

ion population atop the preexisting plasma sheet component, it has been explained as reflection and acceleration of ion populations by the approaching dipolarization front [*Zhou et al.*, 2010, 2011]. Because P5 was at higher latitude than the other probes, the observed reflected ions appear different from those observed by probes at the CPS. As shown in Figure 3f, they appear at around 07:50:20 UT, which is earlier than at other probes. The flux of those reflected ions fade out as the weak DF approaches P5. The enhancement of ion flux that appears even earlier than ~07:50:20 UT may be caused by the small dipolarization prior to the DF and the intermittent reductions of ion flux during this interval may be caused by the motion of spacecraft across the boundary layer. The earlier arrival of these DF-reflected ions suggests an *x*-extended region with enhanced ion fluxes in the earthward direction at higher latitudes. Moreover, the angular distributions of reflected ions are also different from the CPS to the higher latitude. Among the probes in the CPS (P1–P4 in Figures 3b–3e), the ion distributions appear to shift dawnward. Note that the spectra have been recalibrated to ensure that the 0° and 90° angles correspond to the earthward and duskward directions, respectively. This difference has been explained by *Zhou et al.* [2010]. In our companion paper we will further discuss the almost unrestricted streaming of these high-latitude ions along field lines toward the Earth [*Zhou et al.*, 2012]. In Figure 3g, we show the

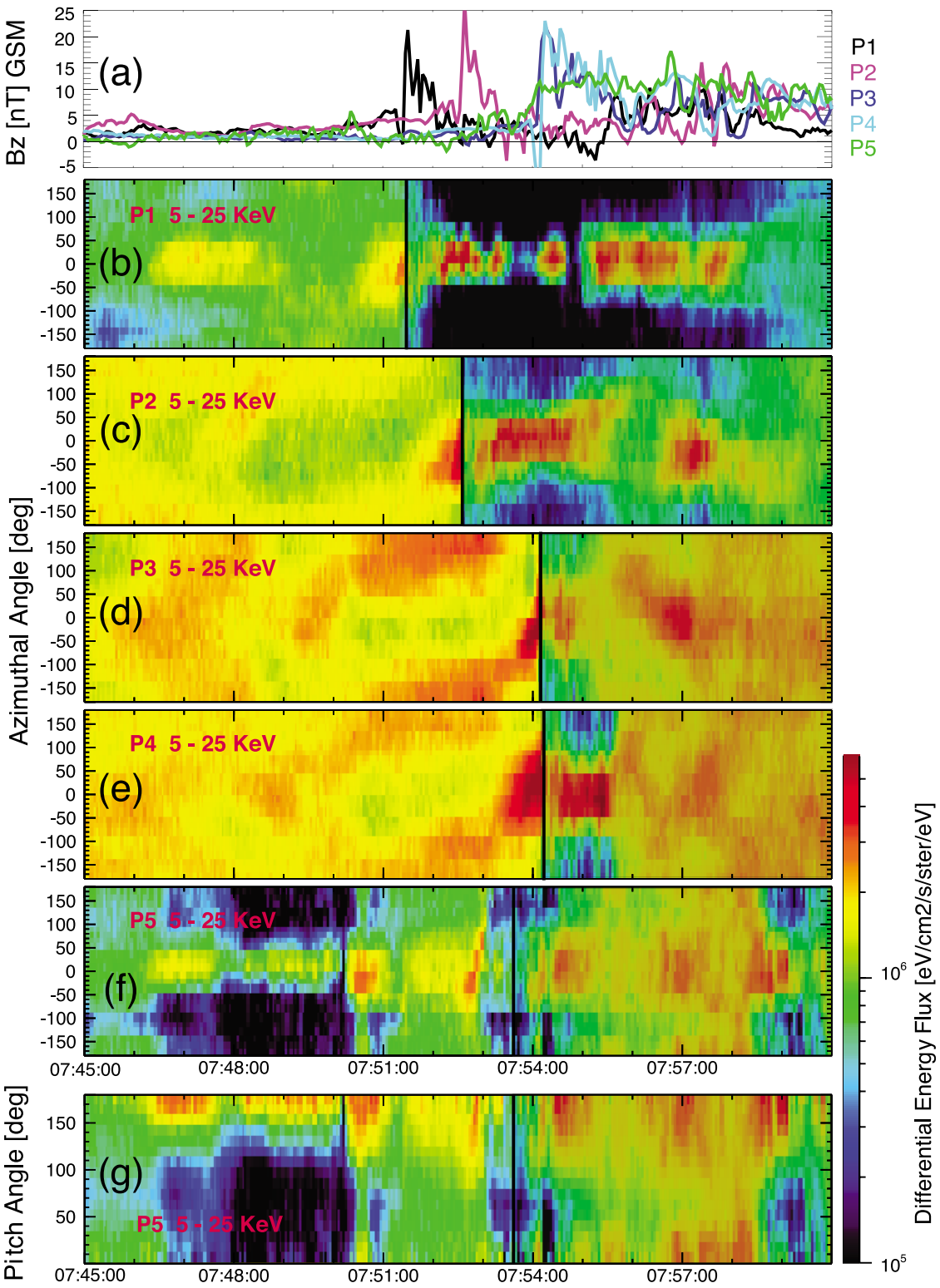


**Figure 3.** (a) The Bz components of the magnetic field, (b–f) the differential energy flux of 5–25 KeV ions versus azimuthal angle observed by THEMIS probes, and (g) the differential energy flux of ions versus pitch angle at P5 during the 27 February 2009 event. The vertical lines mark the arrival times of DF at each spacecraft and the time intervals after DF arrival are shaded.

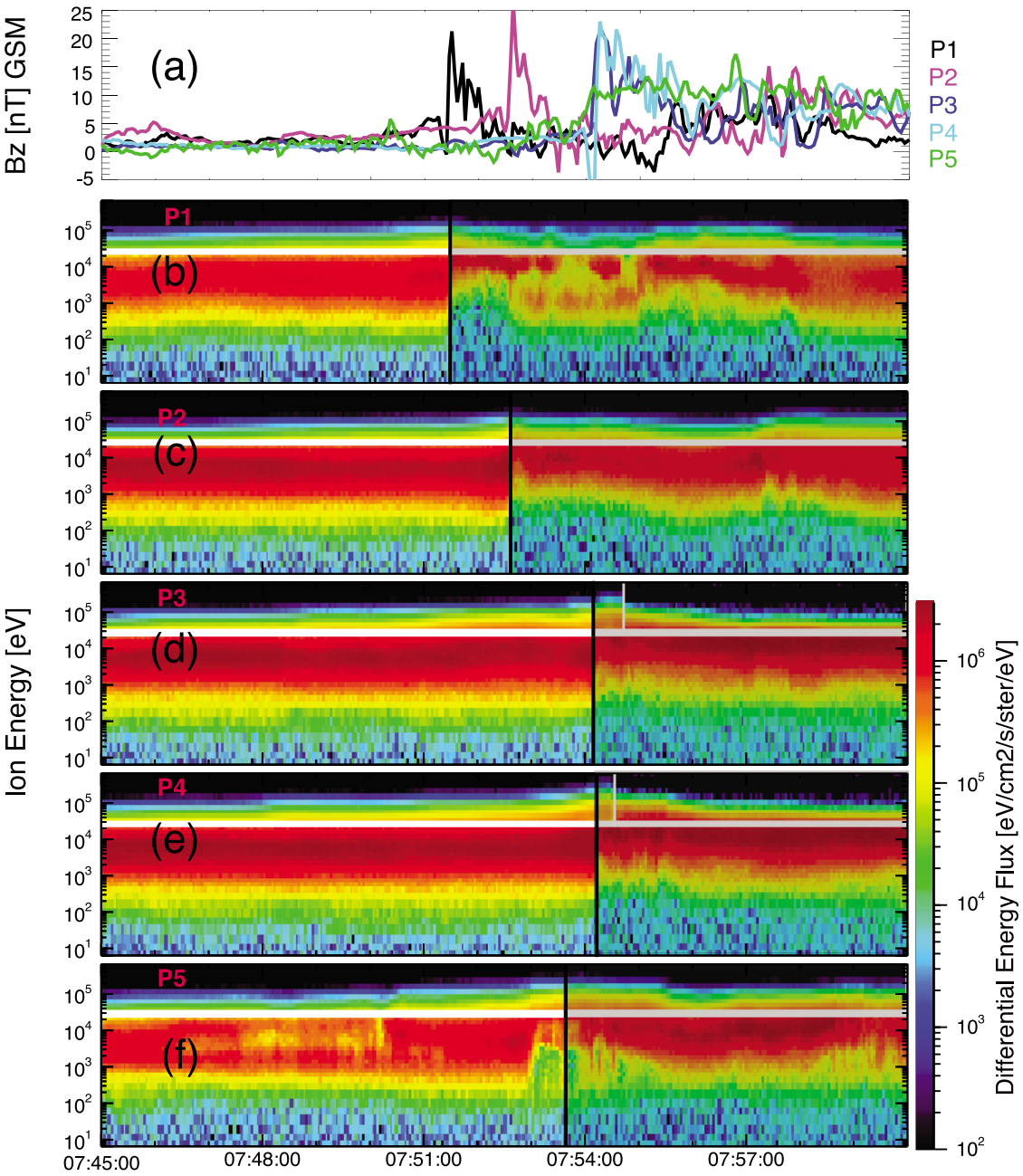


**Figure 4.** (a) The Bz components of the magnetic field and (b–f) the differential energy flux of 5–100 KeV ions observed by THEMIS probes during the 27 February 2009 event. The vertical lines mark the arrival times of DF at each spacecraft and the time intervals after DF arrival are shaded.

differential flux of ions at P5 versus pitch angles. At higher latitudes (P5), the earthward-streaming ions are mostly field-aligned.

[10] In Figure 4, we show the energy spectrum of ions around DFs with the Bz components of the magnetic fields in Figure 4a. In this figure it can be seen that the ion energy starts to rise before DF arrival, suggesting that these ions are also accelerated by the DFs during this reflection process. Similar to the azimuthal angle distributions in Figure 3, the high energy flux at P5 appears to rise earlier than those at P3 and P4, which shows the *x*-extended region of energized ions at higher latitudes and also the limited accessibility region in the CPS.

### 2.2. Dipolarization Front Observations on 18 March 2009

[11] Another event studied in this paper was observed by THEMIS P3, P4, and P5 on 18 March 2009 during a small substorm (maximum AE about 300 nT). Figure 5 shows the orbits and footprints of THEMIS probes in the same format as Figure 1. During this event, THEMIS P1 and P2 are away from the midnight sector and from the CPS. Similar to the orbits in

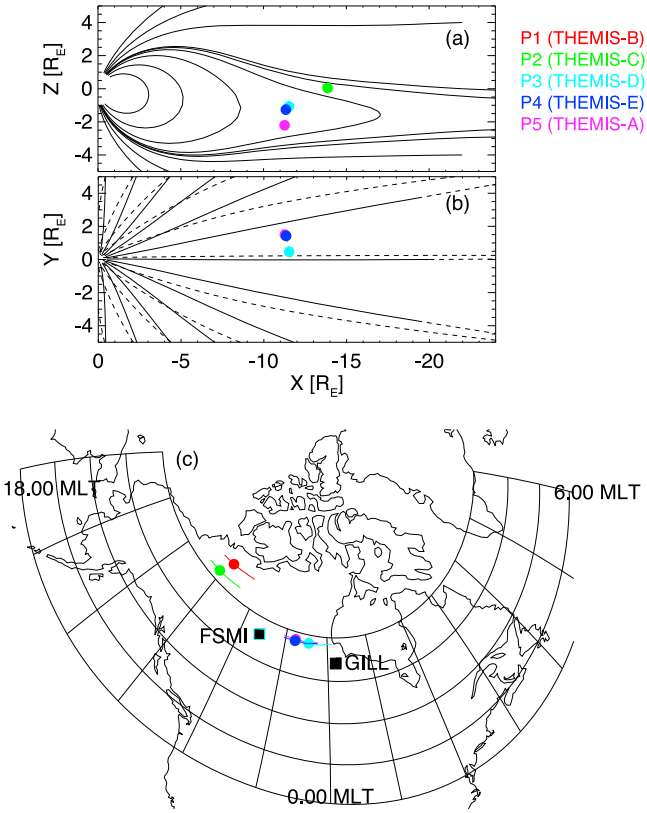


**Figure 5.** The projection of THEMIS probe orbits in the (a) XZ and (b) XY planes with T96 field lines on 18 March 2009; (c) the footprints of THEMIS probes from T96 model mapping.

the February 27 event, P5 is farthest away from the CPS of the three inner probes. P3, P4, and P5 map between the stations FSMI and GILL according to the T96 model (Figure 5c) and their footprints are slightly farther away from FSMI than those of P1, P2 and P5 in the previous event (Figure 1c).

[12] The Bz components of the magnetic field observed by P3, P4, and P5 are shown in Figure 6a. The most prominent and abrupt Bz component change was observed by P4; the dipolarizations at P3 and P5 were relatively gradual. Marked by the minima of the Bz component that are immediately before the most significant Bz enhancements, the arrival times of DF at P3, P4 and P5 are 07:09:41, 07:09:35, and 07:09:42 UT respectively. The Bz component enhancement at the three probes persisted for about 1 minute, followed by a short interval of weak Bz components and multiple dipolarizations. In this event, earthward-reflected ion populations were also seen prior to the DFs by all three probes. Because of this substorm's small magnitude and the relatively quiet ambient plasma sheet, the earthward flux is shown more clearly than in the February 27 event. The reflected earthward ion populations are also clearly seen on the high-energy ions (Figures 6d–6f). Especially at P5, which is at the highest latitude of the 3 inner probes, the earthward population of ions is seen several minutes prior to DF arrival and stands out prominently from the background plasma sheet population. As in the previous event, the reflected ion distributions appear dissimilar at different latitudes. The azimuthal angles of these ions slightly shift toward the dawnward direction in the CPS (P3 and P4), whereas ions observed by P5 are distributed around the earthward direction. The earthward ion flux appears intermittent at P5, similar to the previous event, which is also due to the relative motion of P5 to the boundary layer. The reductions of the earthward ion flux prior to the DF at P5 well correspond to the increases of the Bx magnitude, showing that the spacecraft is farther away from the neutral sheet. This difference again suggests that in the CPS, reflected ions are confined to the limited region ahead of the fronts, whereas ions with dominant Vx components can access higher latitudes and stream along the field lines more freely. In Figures 6d and 6g, there is also a transient reduction in the earthward ion flux after the DF. Figure 6h shows the pitch angle distribution observed at a higher latitude (P5). As in the 27 February event, the reflected ions are mostly along the field lines. In the following sections, we will show that these energized earthward ions are likely responsible for the transient proton auroral intensifications observed by ground meridian-scanning photometers.

## 3. Multispectral Auroral Observations at Fort Smith

### 3.1. CANOPUS MSP

[13] Multispectral auroral observations during the two events were made by the CANOPUS meridian-scanning photometer (MSP) at Fort Smith, Canada (located at 60.00° geodetic latitude, 248.12° geodetic longitude, and roughly 67° geomagnetic latitude). The CANOPUS MSPs are meridian-scanning eight-channel filterwheel photometers. Five of the channels measure auroral emissions (470.9 nm, two at 486.1 nm, 557.7 nm, and 630 nm); the remaining three measure background intensities (480 nm, 493.5 nm, and 625 nm) to correct for contamination by blended auroral emissions and scattered light of solar and/or lunar origin. In this study, we use the 486.1 nm $H_\beta$ line to monitor precipitating protons in the tens of keV energy range. The instrument sweeps through the meridianal sky twice each minute, and each scan is binned into 17 latitude bins. For 470.9 nm, 486.1 nm, and 557.7 nm, bin boundaries are computed assuming an altitude of 110 km and the resulting bins are 0.5 degree latitude wide. For 630 nm, however, the emission altitude is assumed to be 250 km and the resulting bins are 1 degree latitude wide. The MSP azimuths are different, and the MPA (Meridian Photometer Array) azimuth of Fort Smith is about 5.7°.

[14] Due to the limited MSP azimuth, the conjugation between in situ probes and ground stations is usually short. For example, based on the T96 model, P1 was conjugate with Fort Smith MSP from approximately 07:00 to 08:00 UT on 27 February 2009. This conjugation is also shown in Figure 1c, in which the footprint of P1 was about 5° east of Fort Smith when it observed the arrival of the DF. It has to be noted that

**Figure 6.** (a) The Bz components of the magnetic field, (b–g) the differential energy flux of 5–25 KeV and 30–100 KeV ions versus azimuthal angle observed by THEMIS probes, and (h) the differential energy flux of ions versus pitch angle at P5 during the 18 March 2009 event. The vertical lines mark the arrival times of DF at each spacecraft and the time intervals after DF arrival are shaded.

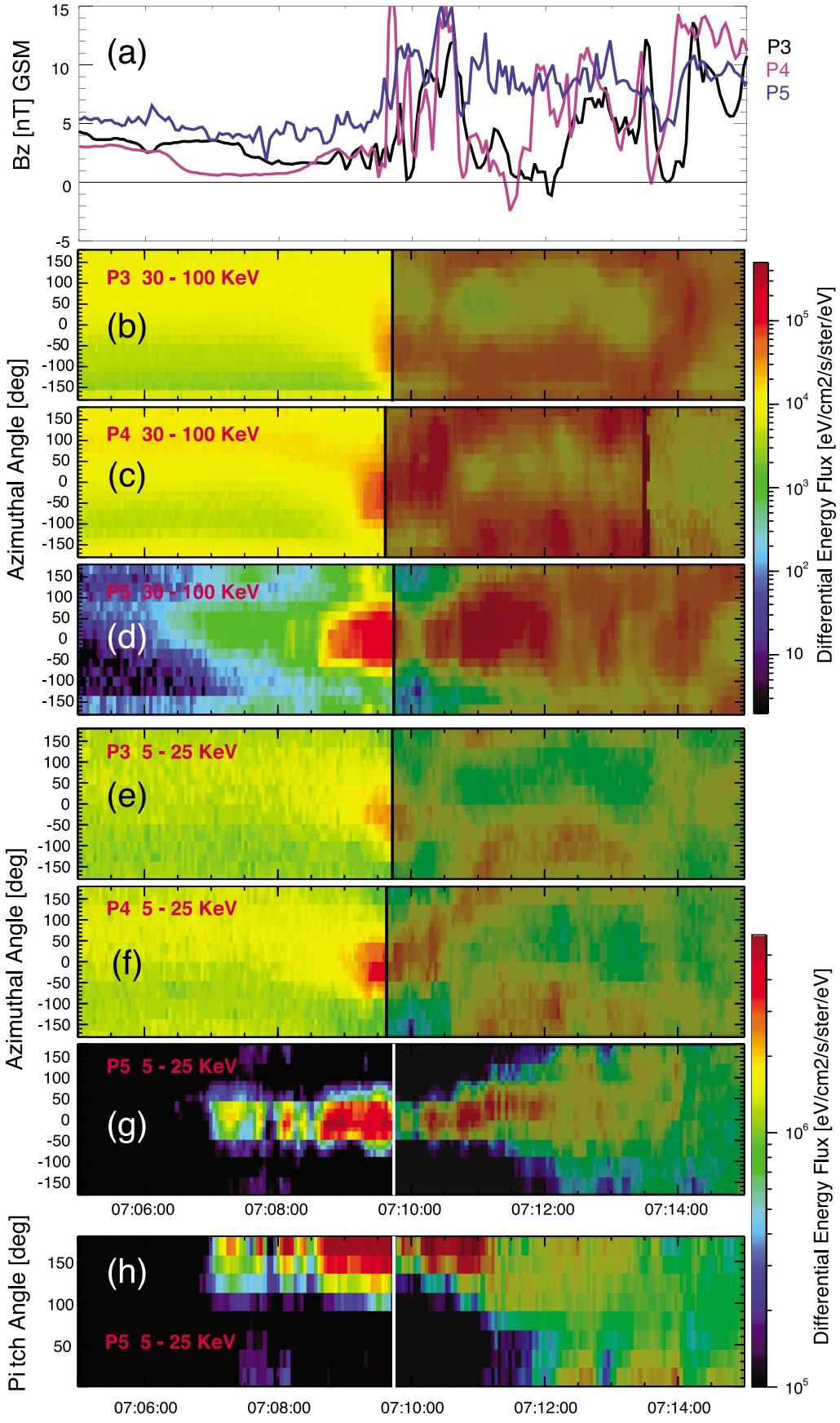
(a)
Bz [nT] GSM
P3
P4
P5
(b)
P3 30 - 100 KeV
(c)
P4 30 - 100 KeV
(d)
P5 30 - 100 KeV
Azimuthal Angle [deg]
Differential Energy Flux [eV/cm2/s/ster/eV]
(e)
P3 5 - 25 KeV
(f)
P4 5 - 25 KeV
(g)
P5 5 - 25 KeV
07:06:00
07:08:00
07:10:00
07:12:00
07:14:00
(h)
P5 5 - 25 KeV
Pitch Angle [deg]

**Figure 6**

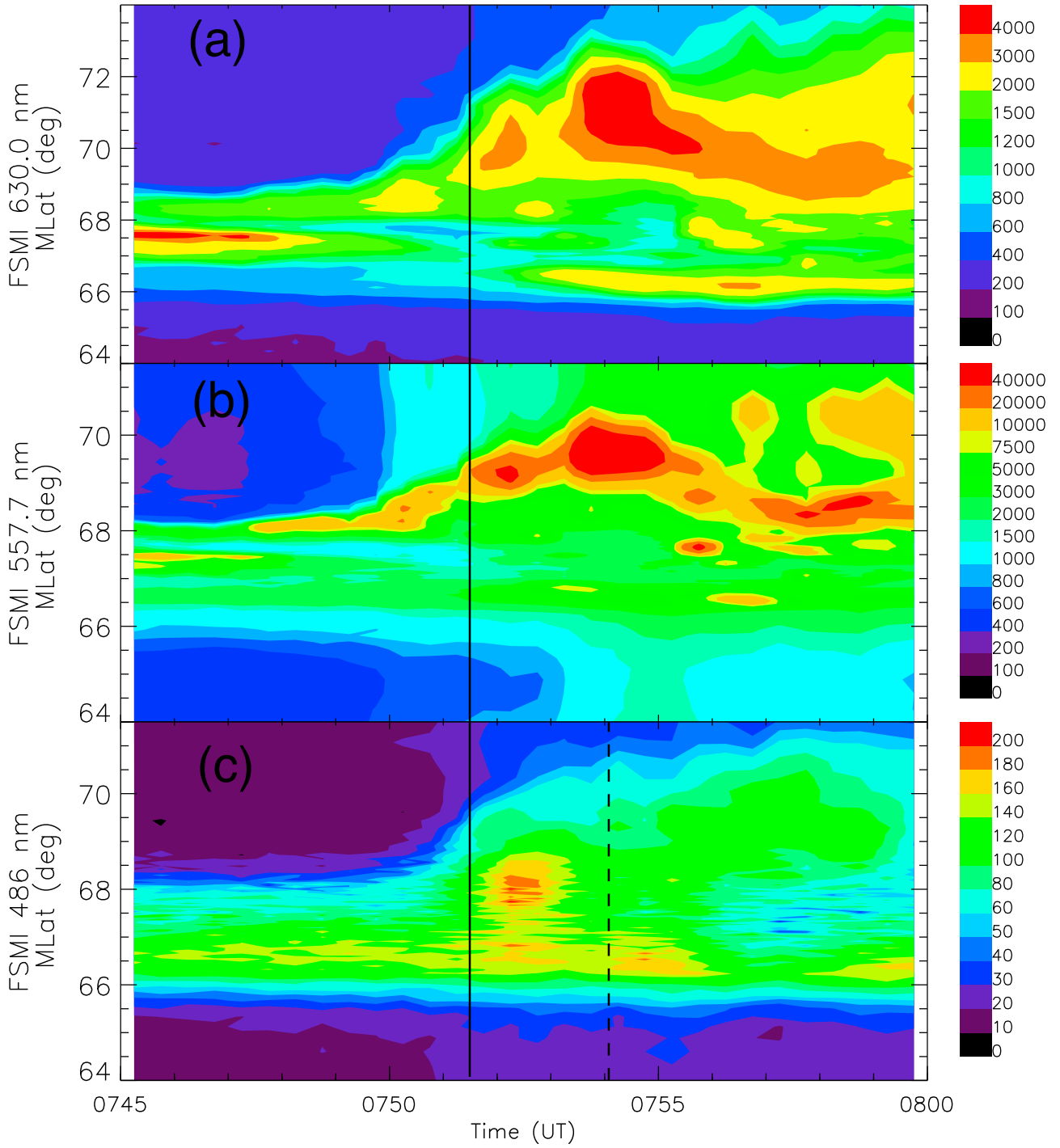


**Figure 7.** The keograms of Fort Smith MSP at different lines for the 27 February 2009 event: (a) 630 nm, (b) 557.7 nm, and (c) 486 nm. Note that the color bars for 630 nm and 557.7 nm are not in linear scale, but that for Figure 7c is in linear scale. The vertical black line marks the time when the DF arrives P1, and the second short dashed line marks the DF arrivals at P3, P4, and P5.

the mapping results from the T96 model have to yield some errors, especially during the active times.

### 3.2. Auroral Keograms From the 27 February DF Event

[15] Figure 7 shows keograms in 630 nm, 557.7 nm, and 486.1 nm wavelengths from the MSP at FSMI after substorm onset and around DF arrival at THEMIS probes. The black vertical line indicates DF arrival time at P1 (07:51:24 UT), the probe that is farthest tailward. The activities of white-light aurora in this event have been discussed elsewhere [*Tang et al.*, 2010; *Ge et al.*, 2011; *Lyons et al.*, 2012; *Runov et al.*, 2011b]. As shown in Figure 7b, the initial brightening of the major breakup in this event started from a new arc

on FSMI at around 07:45 UT, whereas the poleward expansion of auroral brightening did not begin until 07:49:30 UT. The arrival of DFs at THEMIS probe P1 coincided with a strong intensification and further poleward expansion of auroral brightening. In fact, from the observations of THEMIS All-Sky Imagers (ASI) [*Mende et al.*, 2008], this auroral intensification developed further into a north-south (NS) structure reaching about 70° magnetic latitude (see the left panel of Figure 3 in *Runov et al.* [2011b]). It is also found in Figure 7a that the red-line (630 nm) aurora produced by soft-electron precipitation followed a pattern similar to green-line emissions (557.7 nm in Figure 7b). The red-line emissions are located about 2° poleward of the green-line emissions, however.

[16] Figure 7c shows $H_\beta$ emissions, which are used to monitor the proton precipitation/auroras. The proton aurora was also found to intensify after initial brightening of electron auroras at lower latitudes (the intensity peak is located more than 1° equatorward of the electron onset arc). The poleward boundary of the proton auroral belt coincided with the electron onset arc, which is consistent with previous observations [*Takahashi and Fukunishi*, 2001]. The proton auroral belt, which started to expand poleward at around 07:50:30 UT, one minute later than the poleward expansion of electron auroras, was accompanied by further enhancements on the equatorward part of proton auroral belt. However, the fading of proton aurora during the late growth phase was not seen (compare with observations from *Liu et al.* [2007]). Atop the general proton auroral belt expansion and low-latitude intensifications, a remarkably enhanced proton aurora appeared after the first DF arrived at the mid-tail THEMIS probe P1 (07:51:24 UT). This intensified patch reached its peak about 1 minute after the first DF arrival. The peak intensity of this proton auroral patch was abnormally high, up to about 200 Rayleigh (R). It is also very interesting that the peak of enhanced proton aurora patch was located about 2° higher in latitude (centered around the 68.2° magnetic latitude) than the intensity peak of the pre-existing proton auroral belt (66.5°) and appeared to be detached from the equatorward enhancements of proton aurora. This isolated enhancement of proton aurora lasted for about 1.5 min, i.e., 3 complete MSP scans. As indicated in Figure 2 and marked by the short dashed line in Figure 7c, P3, P4, and P5 observed another DF about 2.5 min after arrival of the first [*Lyons et al.*, 2012]. After a short interval of reduction, another enhanced proton precipitation was seen to start at a lower latitude (centered around 66.5° magnetic latitude, the latitude of the intensity peak of pre-existing proton auroral belt). This enhancement of proton precipitation coincides with the arrival times of DFs at THEMIS P3, P4, and P5 (marked by the vertical dashed line at 07:54:09 UT). It is seen from this panel that after the DF arrival at P3, P4 and P5 at ~07:54:10 UT the proton precipitation starts to enhance between the magnetic latitudes 66.2° and 67.1°. This patch persisted for a similar interval, 2 min, which allows the ground-based MSP to completes 4 scans. Although the intensity of this proton auroral patch is lower than the previous enhancement at 07:51:30 UT, the maximum luminosity reaches 180 R which is significantly greater than those of the background and growth-phase proton aurora (120–140 R). The proton precipitation then subsided until another low-latitude intensification appeared at about 07:58 UT.

### 3.3. Auroral Keograms From the March 18 DF Event

[17] The MSP observations on the March 18 DF event (also from FSMI) are shown in Figure 8, which has the same format as Figure 7. In Figures 8a and 8b and the white-light keograms at FSMI and Snap Lake (not shown here), initial substorm brightening can be seen to start at roughly 07:08:40 UT; substantial intensification and poleward expansion began approximately one minute later (coinciding with DF arrival at THEMIS P3, P4, and P5). The latitude of the proton aurora intensity peak was also generally 1.5° lower than the electron onset arc, and again, in contrast to the observations in *Liu et al.* [2007], the proton aurora did not appear to fade prior to substorm onset. The black vertical line in Figure 8 marks the arrival of DFs at THEMIS P3, P4, and P5 at around 07:09:35 UT. As shown in Figure 8c, a transient, latitude-elongated $H_\beta$ emission enhancement appears after the DFs were observed in the equatorial plane by THEMIS probes. Because of the substorm's smaller magnitude (maximum AE of this substorm is about 300 nT), auroral luminosities at all spectral lines are significantly lower than those in the February 27 substorm. However, the proton auroral enhancement in the March 18 event is similar to the second enhancement found in the February 27 event that coincides with the arrival of the second DF at the inner THEMIS probes (P3 and P4). The enhancement's intensity peak is located at the same latitude of the late growth-phase proton auroral belt, and the poleward boundary of the proton auroral belt extends outside of the field-of-view of FSMI MSP. In this event, the maximum intensity of $H_\beta$ emissions only reaches 90 R, significantly lower than that in the February 27 event (200 R). The transient proton auroral enhancement lasts approximately 2 min, the length of about 4 complete MSP scans. It is noteworthy that in this event, the transient proton auroral enhancement appears slightly earlier than the main electron auroral intensifications on both the red and green lines. This time delay can be explained by the larger longitudinal separation between the THEMIS probe footprints and FSMI in this event than in the February 27 event (Figures 1c and 5c). It will take longer for electron precipitation to move into the field of view of FSMI MSP than for the protons because plasma sheet protons move rapidly in the westward direction due to westward drifting in the near-Earth region. Westward motion of electron auroras, however, depends mainly on the general westward motion of the entire auroral brightening source region. The general westward motion of electron aurora is also found on the All-Sky Imager at FSMI, which suggests that the particle precipitation source region was initially located east of the azimuth of FSMI.

[18] An important difference between the proton auroral variations in this event and those in the February 27 event is that in this event there is a clear proton precipitation dropout about 2 min after transient enhancement, whereas in the February 27 event, there is only a small reduction in proton aurora after the first intensification. The intensity of proton aurora during this dropout is even lower than that of growth-phase proton aurora, and this proton aurora dropout coincides with the time when the peak intensity of electron auroras occurred. The enhanced, expanded proton auroral belt appears after this dropout and further intensifies for the next 15 minutes. It is noted that this transient dropout of proton aurora during the substorm expansion phase, which is

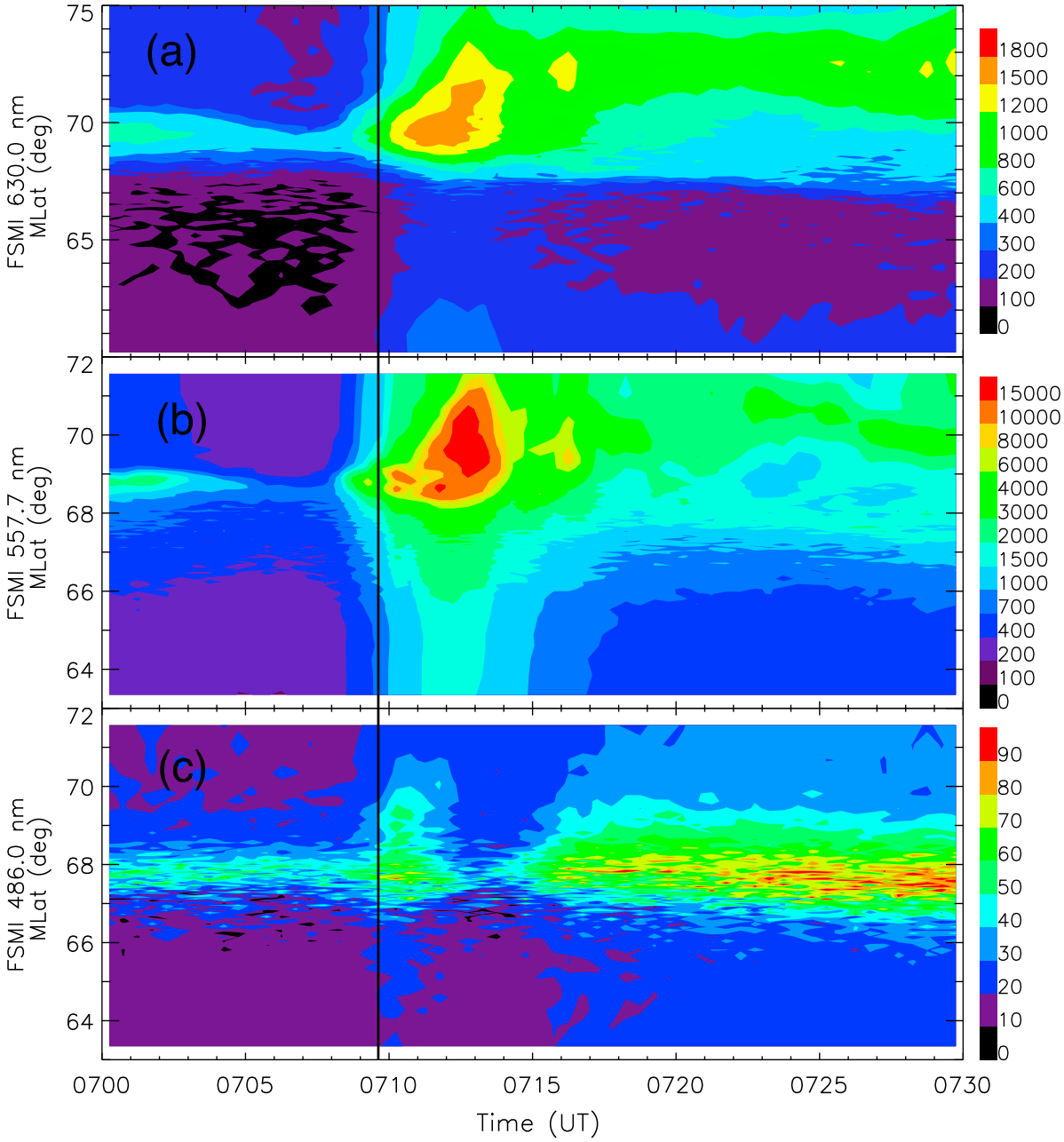


**Figure 8.** The keograms of Fort Smith MSP at different lines for the 18 March 2009 event in the same format as Figure 7.

different from the fading during the later growth phase [*Liu et al.*, 2007], is hardly mentioned previous studies on proton auroras. It is interesting that in Figure 6 the earthward ion population flux variations have a pattern similar to proton auroral variations but with about 2 min time difference. This pattern is especially prominent at THEMIS P5, which at this time was farther from the CPS than P3 and P4. Earthward ion flux variations immediately after DF arrival can be seen more clearly in Figures 6d and 6g. The Bz components that correspond to this reduction in earthward ion flux were found to be very strong in the dipolarization region. Although those components were highly perturbed at all three probes, (Figure 6a), the general trend of the Bz variations is similar at all probes (the Bz components increase strongly after the DF and dipolarizations last approximately one minute). Multiple dipolarizations were seen at all three probes for ten minutes after the first DF.

## 4. Summary of Conjugate Observations and Implications

[19] In above sections we have presented two examples of conjugate dipolarization front observations. During two DF events, the ground MSP was magnetically conjugate with THEMIS probes in the plasma sheet. These rare conjugations enable us to obtain simultaneous observations of multiple-spectrum auroras and in situ particle distributions and magnetic field variations of DFs. In these two events, ions that

**Table 1.** Timing of DF and Proton Auroral Intensification[a]

| Events | $T_{ion}$ | $T_{DF}$ (S/C:POS) | $T_{P0}$ | $T_{P1}$ | $MLat_P$ |
|---|---|---|---|---|---|
| 02/27/2009 E1 | 07:50:25 UT | 07:51:25 UT (P1: [−16.7, −1.6, −2.2]) | 07:51:25 UT | 07:53:25 UT | 68.0° |
| 02/27/2009 E2 | 07:53:10 UT | 07:54:09 UT (P4: [−11.1, −1.8, −2.4]) | 07:54:10 UT | 07:56:10 UT | 66.5° |
| 03/18/2009 | 07:08:50 UT | 07:09:35 UT (P4: [−11.4, 1.3, −1.3]) | 07:09:40 UT | 07:12:00 UT | 67.6° |

[a]$T_{ion}$: Start time of earthward ion flux enhancement; $T_{DF}$ (S/C:POS): Arrival time of dipolarization fronts (spacecraft name: position in GSM coordinates); $T_{P0}$/$T_{P1}$: Start/Stop time of proton aurora enhancement; $MLat_P$: the latitude of the peak intensity of the proton aurora enhancement.

were reflected and energized by approaching DFs appeared to be directed earthward in the DF precursor flow region. After the earthward ions were observed by THEMIS probes, the ground MSP recorded transient proton precipitation enhancements atop the intensification and expansion of the proton auroral belt during substorm expansion phases. In the February 27 event, the first enhanced proton auroral patch appeared at higher latitudes and was detached from the equatorward main peak of the proton auroral belt after the first DF event was observed by P1, the middle-tail THEMIS probe, at 21 $R_E$ downtail. When another DF event arrived at the inner probes, P3 and P4, the second isolated proton precipitation enhancement was seen at a lower latitude, close to that of the equatorward peak of the proton auroral belt. In another DF event during the substorm on 18 March 2009, transient proton precipitation enhancements were also found at FSMI after DF arrival at THEMIS P3, P4, and P5, about 2 min prior to major electron auroral intensifications. The proton auroral intensification peak appeared at the same latitude as the growth-phase proton aurora, which quickly expanded poleward after substorm onset. A remarkable $H_\beta$ emission dropout after transient enhancements found for the March 18 event is consistent with dropout of the earthward ions at THEMIS probes with about 2 min time delay. We summarize the above observations in Table 1, where the start times of earthward ion flux, arrival times of DFs at different probes, the start/stop times of the proton aurora intensifications, and the magnetic latitudes of the intensity peak of proton aurora are listed. From the three events studied here, it can be clearly found that the ground-observed proton aurora enhancements appear about 1–2 min after the earthward ion flux enhancements observed by THEMIS spacecraft and the latitudes of the observed auroral intensifications are well correlated with the locations of DFs.

[20] From the above observations, we postulate that the earthward population of ions reflected and energized by approaching DFs is the source of ground-observed proton auroral enhancements and that interaction between earthward-propagating DFs and the ambient plasma sheet provides another mechanism to accelerate and re-distribute plasma sheet ions other than magnetic reconnection in the magnetotail. Our companion paper investigates acceleration and reflection of plasma sheet ions as DFs pass through the plasma sheet and discusses how these earthward ions move and the probability of their precipitating into the ionosphere [*Zhou et al.*, 2012]. Briefly, these DF-reflected ions near the PSBL (e.g., ions observed by THEMIS P5), energized to the energy range from several to a few tens of keV, stream along field lines and eventually generate proton auroral enhancements in the ionosphere. Although the DF-plasma sheet interaction occurs continuously along with earthward DF propagation, the corresponding proton auroral enhancements may appear transient in the MSP field of view because the local time of the interaction region may change during earthward propagation. The latitudes of DF-associated proton precipitation are determined by the distance of the source region from Earth when the source region becomes magnetically conjugate with the ground MSP.

[21] Moreover, we find that source ion reduction can also cause a decrease in proton precipitation into the ionosphere. In the March 18 event a significant proton precipitation dropout corresponds earthward ion flux reduction (shown in Figure 6). The earthward ion flux reduction after the DF can be attributed to relaxation of the compression produced by the fast flow. After the DF (after 07:10:30 UT), the plasma flows observed by P3 and P4 turned tailward and dawnward. As a result, plasma sheet compression was relaxed due to plasma flow diversion and reflection, which also caused ion reflection to cease. In Figures 6d and 6g we see that after this transient reduction, earthward ion flux again rose, which are associated with the following earthward-moving DFs seen at P3 and P4.For example, the dipolarization fronts observed by P4 at ∼07:11:50 UT, ∼07:12:15 UT, and at around 07:13:30 UT (Figure 6a) might be able to produce these earthward ion populations. It is noteworthy that the luminosity of $H_\beta$ emissions during the dropout is even lower than in the growth phase, which can be explained by the reduction in proton precipitation from the background plasma sheet. Since sufficient pitch angle scattering in the stretched magnetic field is required for typical proton precipitation in the plasma sheet, the absence or reduction of proton aurora is often seen when the tail magnetic field is dipolarized. For example, *Gilson et al.* [2011] statistically studied large-scale proton precipitation reduction during substorms and found that clear proton aurora splitting is observed in about half the events they considered. In their recent paper [*Gilson et al.*, 2012], proton auroral splitting (or reduction/absence) is shown to be caused by penetration of dipolarization regions into the inner plasma sheet. Thus, significant proton auroral dropout after DF-associated enhancements could also be caused by a dipolarization region of limited size following the DF and further reducing background plasma sheet precipitation. Because of the diffuse nature of proton aurora, such dynamic proton auroral variation may not be caused by global temporal change in tail configuration but by passage of spatial DF-related structures over the meridian of FSMI MSP.

## 5. Global MHD Simulation Perspective

[22] The February 27 substorm has been extensively studied by many authors [e.g., *Runov et al.*, 2009; *Tang et al.*, 2010]. Using the global MHD simulation model OpenGGCM, *Ge et al.* [2011] simulated this substorm event to study the formation of DFs and their relation to substorm auroral breakups. In their study, the key signatures of this substorm, including DFs, BBFs, and aurora breakups, are well reproduced. In this

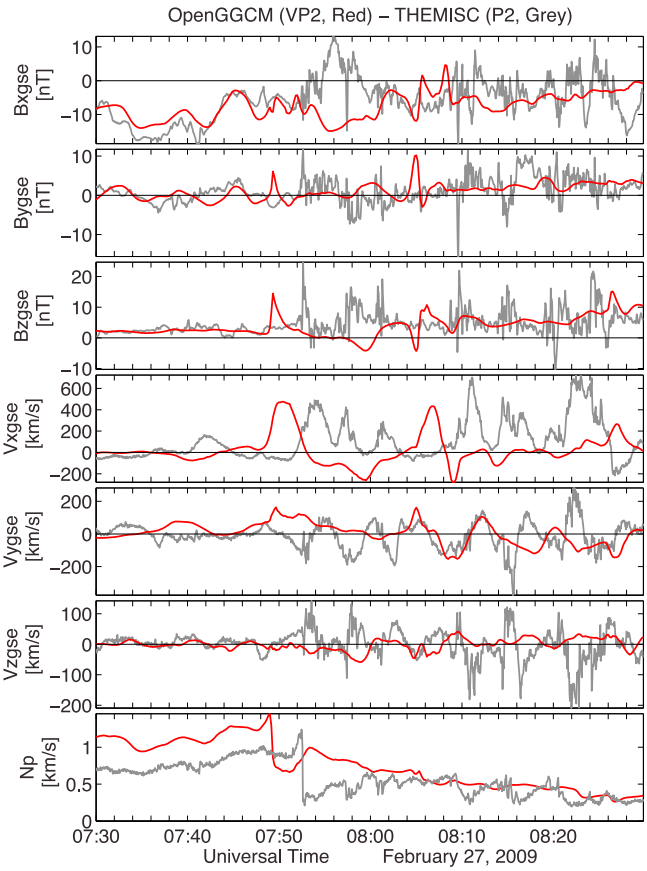


**Figure 9.** Comparison of the MHD state variables measured by P2 (black lines) with those from the OpenGGCM simulations VP2 (red lines). From top to bottom, the panels show the three components of the magnetic field, the three components of plasma velocity, and the plasma number density.

paper, we use these simulation results to further investigate proton precipitation during the earthward propagation of DFs. In this section, we will summarize the global MHD simulation results for this substorm and then show our simulated proton precipitation using the Field-Line-Curvature (FLC) model.

### 5.1. Summary of Simulation Results of February 27 Substorm and DFs

[23] The global MHD model OpenGGCM reproduced many key features of the February 27 substorm, including the dipolarization fronts. Adapted from Figure 9 in *Ge et al.* [2011], Figure 9 replots the time series of the magnetic field and plasma parameters from both simulation results (red traces) and THEMIS in situ observations (gray traces), where VP2 represents the virtual satellite in our simulation with positions similar to those of P2. To obtain better agreement between the time series in our simulation and observations, we made slight adjustments to the positions of the virtual satellites, e.g., moved VP2 slightly southward. At 07:49 UT, P2 was located at [−16.72, −2.08, −1.72] $R_E$ in GSE coordinates, and VP2 is 1.0 $R_E$ below P2. In Figure 9, we can see that the magnetic field variations generally match THEMIS observations. In particular, Bz component variations around DF are reproduced about 4 min earlier than the observed DF, including the small decrease in the Bz component prior to the DF. As in the observations, this DF is accompanied by a strong earthward BBF and substantial plasma density changes, including a rapid increase prior to the DF. It must be noted, however, that the thickness of the simulated DFs is significantly greater than that in the observations. Although the thickness of DF becomes smaller along the earthward propagation of this structure, i.e., the DF becomes steeper, the steepest DF still has a thickness of 2–3 grid cells across, suggesting that simulation becomes under-resolved by the simulation grid-size [see *Ge et al.*, 2011, Figure 15].

[24] The OpenGGCM produces the energy flux and the mean energy of two precipitating electron populations, the thermal electron flux from the inner magnetosphere and electrons that have been accelerated in regions of upward field-aligned current (FAC) [*Raeder et al.*, 2008]. These two populations represent the diffuse aurora and the discrete aurora. In this study, we also calculate the proton precipitating flux to represent the proton aurora. Figure 10a shows a simulated discrete electron aurora during the substorm expansion phase (07:51 UT). In this simulation major electron auroral expansion north of FSMI is reproduced. Figure 10b shows a map of magnetospheric flows made in the central plasma sheet plane determined in our simulations by the maximum of $\beta$ (the ratio of plasma pressure to magnetic pressure), i.e., at the center of the current sheet. The plasma flow vectors are shown in blue/magenta for the tailard/earthward flows. The black contour lines show the Bz distribution in the central plasma sheet. The locations where auroral-brightening regions map into the tail plasma sheet plane are indicated by discrete, solid, color-coded circles; the orbits of virtual satellites are also shown (VP1 - red square; VP2 - green circle; VP3 - cyan triangle; VP4 - blue diamond; VP5 - magenta square). The auroral intensification region at 07:51 UT maps into a broad region along the west edge of the earthward BBF channel on the CPS plane, clearly indicating a relationship between the tail BBF and the major substorm expansion. Penetration of this strong BBF also produces the DFs in our simulation. Figure 10c shows the color contour of the Bz component at the same equatorial plane and the flow pattern. In this simulation, DF variations are produced at the head of the BBF, and the front is located between the enhanced Bz region (dipolarization region) and the preceding weak Bz field.

### 5.2. Simulated Proton Aurora and Relation to DFs

[25] From the results of this simulation, we calculate the proton precipitation energy flux using the FLC model, which assumes that proton precipitation at the nightside ionosphere is caused mainly by pitch angle scattering in the stretched magnetotail. When the average particle gyroradius $\rho$ is sufficiently larger than the radius of the field line curvature (Rc), it is assumed that pitch angle scattering will fill the loss cone. The criteria for sufficient scattering given by *Sergeev et al.* [1983] is $0 < \kappa \leq \sqrt{8}$, where $\kappa = \sqrt{\frac{Rc}{\rho}}$. Adapted from the thermal electron precipitation formula in OpenGGCM [*Raeder et al.*, 2008], the formula for the diffuse proton precipitation energy flux is

$$F = 2f(\kappa)n_i k_b T_i \sqrt{k_b T_i / 2\pi m_i} \quad (1)$$

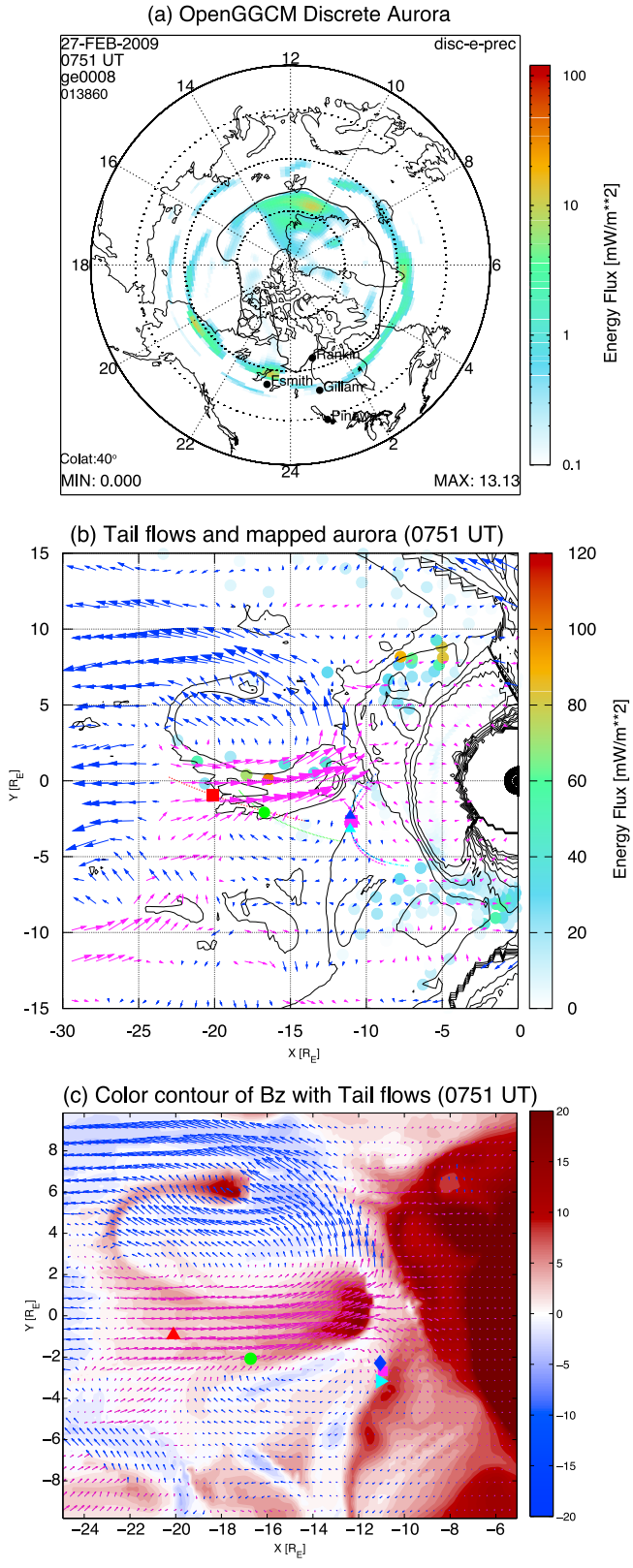


**Figure 10.** Summary of OpenGGCM simulation results for the 27 February 2009 event. See details in the text.

where $n_i$, $T_i$, and $m_i$ are the ion number density, temperature, and mass, respectively; $k_b$ is the Boltzmann constant; $\kappa$ is calculated in the CPS from the MHD variables assuming a simple Maxwellian particle distribution; and $f(\kappa)$ equals 1 when $0 < \kappa \leq \sqrt{8}$. This method, which was used by *Gilson et al.* [2012], can reproduce proton auroral variations observed by the IMAGE-spacecraft. In this study, we use this algorithm to investigate proton auroral variations associated with DFs.

[26] Figures 11a and 11b are the synthetic keograms of discrete electron precipitation and proton precipitation at Fort Smith produced by the OpenGGCM simulation. These keograms are produced by interpolating the global particle precipitation into the longitude of FSMI and into latitudinal grids with 0.1° resolution. Two vertical lines mark times prior to (07:50 UT) and after DF arrivals at the inner THEMIS probes P3, P4 and P5 (~07:53 UT), respectively. From Figure 11a, we find that the discrete electron aurora has begun to intensify and the auroral belt starts to expand both poleward and equatorward, which is consistent with the substorm expansion phase (see Figure 7a). Also shown on Figure 10a, an auroral bulge forms and expands poleward at 07:51 UT. The simulated proton aurora is found to be equatorward of the discrete electron aurora in Figure 11b, consistent with the observations. However, the latitude of the simulated proton aurora belt is about 0.5° poleward of the peak of the observed proton aurora belt. At slightly higher latitudes (around 69.6°), the proton precipitation is also found to intensify after DF arrival. The intensification can be seen immediately after the DF arrives at the near-Earth tail region (the first vertical line in Figures 11a and 11b), from the magnetic latitude of 69.6°. The slight intensification moves equatorward due to the earthward penetration of the DF. However, in our simulations, this intensification of proton precipitation is much less substantial than that observed. This may be due to very little energization of precursor plasma during the interaction between DFs and the ambient plasma in our MHD simulations. This intensification can be better viewed in Figures 11c and 11d, in which the global distribution of proton precipitation in the ionosphere is plotted at two times. Comparing these two panels, we find that proton precipitation near FSMI (shown as Fsmith in Figures 11c and 11d) is clearly enhanced after the DF and the BBF penetrate the inner magnetosphere and the intensifications appear mainly around FSMI and in the region between FSMI and Gillam. The proton auroral belt also slightly expands poleward.

[27] To investigate the source of proton precipitation enhancements, we trace the field lines from the ionosphere to the CPS as we did for the discrete electron aurora (Figure 10b) and show the map of proton precipitation in Figures 11e and 11f at two times. For reference, we show conjugate locations of Fort Smith (black square) and Gillam (purple triangle) in the equatorial plane. In Figure 11f, we see that the enhanced proton precipitation comes from the region in front of the earthward BBF, where the DF is found in our simulations. Major proton precipitation intensification occurs between the meridians of FSMI and Gillam and mainly inside 10 $R_E$, which is consistent with the ionospheric distribution of proton precipitation enhancements. Closer inspection of the CPS shows that the plasma pressure is enhanced in the source region of proton auroral enhancements during DF propagation. This

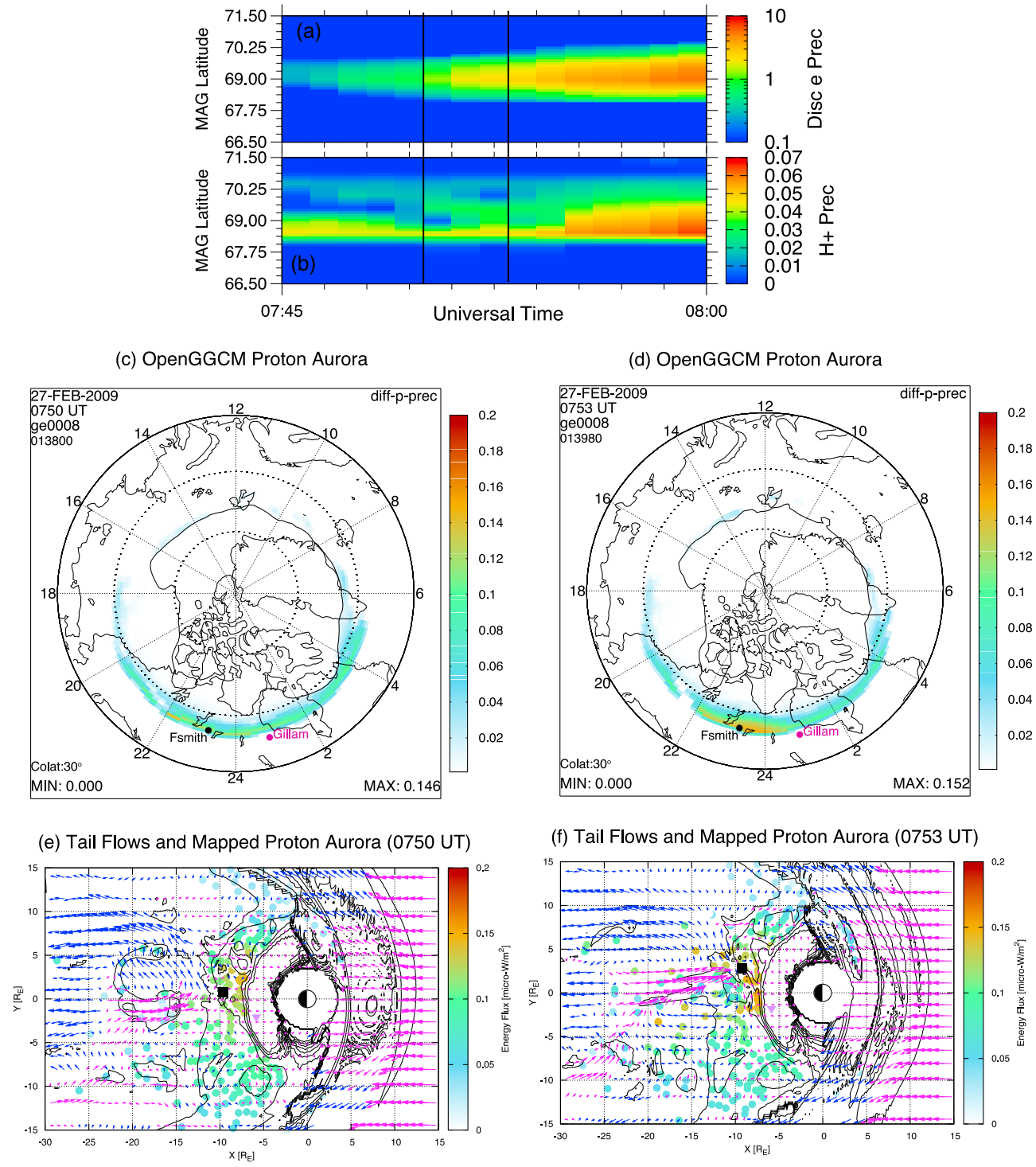


**Figure 11.** Overview of OpenGGCM simulations on proton precipitation during 27 February 2009 event. Simulated keograms of (a) discrete electron and (b) diffuse proton precipitation at Fort Smith. The polar view of the northern hemisphere with color-coded distribution of proton precipitation at (c) 07:50 UT and (d) 07:53 UT. The projections of flow vectors and mapped proton precipitation on the CPS plane at (e) 07:50 UT and (f) 07:53 UT. The mapped locations of Fort Smith and Gillam are shown by the black square and the purple triangle respectively.

pressure enhancement can also be seen in the time series in the seventh panel of Figure 9. The rapid increase in plasma density prior to the DF is very similar to plasma density variations observed by THEMIS probes. In our simulation, this density increase ahead of the DF is the major contributor to plasma pressure enhancement and enhanced proton precipitation because the plasma temperature in this region does not change substantially. The plasma density increase in front of the

earthward BBF and DF is caused mainly by compression of the pre-existing/background plasma on the path of BBF and DF. In our MHD simulations, this compression is consistent with reflection of ions by approaching DFs. In our resistive MHD simulation, however, particle energization or plasma heating by DFs is not present because most dissipation occurs in regions where the resistivity is relatively large, e.g., the diffuse region of magnetic reconnection. We will further investigate energization of reflected ions by DFs in our companion paper using theoretical analysis and test-particle simulations [*Zhou et al.*, 2012].

## 6. Conclusions and Discussion

[28] In this study, we investigate ion dynamics ahead of earthward-propagating dipolarization fronts in two THEMIS-observed substorm events. Enhanced earthward-centered ion distributions in the precursor flow of BBFs are discussed. This type of ion distribution has been attributed to reflection and energization of plasma sheet ions by approaching DFs [*Zhou et al.*, 2011]. An extended investigation of the dynamics of this ion population will also be done in our companion paper [*Zhou et al.*, 2012]. In that paper, we will show that ion DF-reflection, another plasma sheet ion-acceleration process in addition to those caused by magnetic reconnection or by non-adiabatic particle orbits, also changes the pitch angles of plasma sheet ions.

[29] An important observation reported in this study is ground-observed variations of auroral activity associated with magnetotail DFs. Good conjugations between the ground MSP at Fort Smith and THEMIS probes during the events studied in this paper enable us to investigate the effects of the observed ion population reflected by DFs. From ground MSP observations, we find that enhanced proton precipitation appears after DFs arrive at THEMIS probes. An isolated high-latitude proton auroral enhancement is found after the DF observed by the mid-tail probe of THEMIS, P1; proton auroral enhancements at lower latitudes are found to correspond to DFs arriving at the inner probe in both events. A substantial proton precipitation dropout, also found after the DF-associated enhancement in the 18 March 2009 event, corresponds to a similar reduction in earthward ion flux observed by THEMIS probes. This proton precipitation depletion is caused by reduction of both the earthward ions from the DF-reflection process and the background precipitation in the dipolarized field after the DFs. Based on these observations, we postulate that the THEMIS-observed earthward-distributed ions ahead of DFs are the source of the transient proton precipitation enhancements observed by the ground MSP. The interaction between earthward-propagating DFs and the ambient plasma produces reflection and energization of the ions along the paths of DFs and BBFs. During this process, a population of ions mainly distributed in the earthward direction is produced ahead of DFs. Depending on their Vx components after reflection, these ions can access higher latitudes and form an *x*-extended region of field-aligned population that can stream along the field lines toward the ionosphere and produce proton precipitation enhancements. The latitudes of the MSP-observed proton auroral intensifications depend on the geocentric distance of this source region when it becomes magnetically conjugate with the MSP meridian. In our companion paper, we will test this conjecture by examining the behavior of the reflected population of ions and the conditions under which they precipitate into the ionosphere.

[30] We also re-examine our previous global MHD simulation results to calculate the proton precipitation associated with DFs. Using the FLC model, we find that the proton precipitation produced in our simulation also shows enhancements near Fort Smith as the DF propagates earthwards. With real-time field line tracing, we investigate the magnetospheric source of the simulated proton aurora intensifications, and we find that it is located in front of a strong earthward BBF where the DFs are produced in our simulation. The enhancement of simulated proton precipitation is caused by compression of plasma ahead of the earthward penetrating BBFs. In our resistive MHD model, however, the compression mainly causes plasma density increase in that region, but no heating or energization of particles. Understanding the energization process of plasma sheet ions by DFs then requires test-particle simulations, such as those preliminarily performed in our companion paper based on an analytical model of the magnetotail. Test-particle simulations based on the global MHD simulation fields will be performed elsewhere.

[31] **Acknowledgments.** This research was supported by NASA grant NAS5-02099. Development of the OpenGGCM has been supported by NASA grant NNG05GM57G and NSF grant ATM-0639658. Part of the simulations were performed at the National Center for Supercomputer Applications. We thank S. B. Mende, C. T. Russell and THEMIS GBO team, and CANMOS team for providing the ground All-sky-imager data and magnetic field data.

[32] Masaki Fujimoto thanks Christopher Cully and another reviewer for their assistance in evaluating this paper.

## References

Angelopoulos, V., W. Baumjohann, C. F. Kennel, F. V. Coroniti, M. G. Kivelson, R. Pellat, R. J. Walker, H. Luhr, and G. Paschmann (1992), Bursty bulk flows in the inner central plasma sheet, *J. Geophys. Res.*, *97*(A4), 4027–4039.

Angelopoulos, V., C. F. Kennel, F. V. Coroniti, R. Pellat, M. G. Kivelson, R. J. Walker, C. T. Russell, W. Baumjohann, W. C. Feldman, and J. T. Gosling (1994), Statistical characteristics of bursty bulk flow events, *J. Geophys. Res.*, *99*(A11), 21,257–21,280.

Angelopoulos, V., et al. (2008), First results from THEMIS mission, *Space Sci. Rev.*, *141*, 453–476, doi:10.1007/s11214-008-9378-4.

Birn, J., J. Raeder, Y. L. Wang, R. A. Wolf, and M. Hesse (2004), On the propagation of bubbles in the geomagnetic tail, *Ann. Geophys.*, *22*(5), 1773–1786.

Deehr, C., and D. Lummerzheim (2001), Ground-based optical observations of hydrogen emission in the auroral substorm, *J. Geophys. Res.*, *106*(A1), 33–44.

Donovan, E. F., B. Jackel, R. Strangeway, and D. Klumpar (2003a), Energy dependence of the latitude of the 1–25 KeV ion isotropy boundary, *Sodankyla Geophys. Obs. Publ.*, *92*, 11–14.

Donovan, E. F., B. J. Jackel, I. Voronkov, T. Sotirelis, F. Creutzberg, and N. A. Nicholson (2003b), Ground-based optical determination of the b2i boundary: A basis for an optical MT-index, *J. Geophys. Res.*, *108*(A3), 1115, doi:10.1029/2001JA009198.

Fukunishi, H. (1975), Dynamic relationship between proton and electron auroral substorms, *J. Geophys. Res.*, *80*(4), 553–574.

Galand, M., and S. Chakrabarti (2006), Proton aurora observed from the ground, *J. Atmos. Sol. Terr. Phys.*, *68*(13), 1488–1501, doi:10.1016/J.Jastp.2005.04.013.

Ge, Y. S., J. Raeder, V. Angelopoulos, M. L. Gilson, and A. Runov (2011), Interaction of dipolarization fronts within multiple bursty bulk flows in global MHD simulations of a substorm on 27 February 2009, *J. Geophys. Res.*, *116*, A00I23, doi:10.1029/2010JA015758.

Gilson, M. L., J. Raeder, E. Donovan, Y. S. Ge, and S. B. Mende (2011), Statistics of the longitudinal splitting of proton aurora during substorms, *J. Geophys. Res.*, *116*, A08226, doi:10.1029/2011JA016640.

Gilson, M. L., J. Raeder, E. Donovan, Y. S. Ge, and L. Kepko (2012), Global simulation of proton precipitation due to field line curvature during substorms, *J. Geophys. Res.*, *117*, A05216, doi:10.1029/2012JA017562.

Hwang, K. J., M. L. Goldstein, E. Lee, and J. S. Pickett (2011), Cluster observations of multiple dipolarization fronts, *J. Geophys. Res.*, *116*, A00I32, doi:10.1029/2010JA015742.

Liu, W. W., E. F. Donovan, J. Liang, I. Voronkov, E. Spanswick, P. T. Jayachandran, B. Jackel, and M. Meurant (2007), On the equatorward motion and fading of proton aurora during substorm growth phase, *J. Geophys. Res.*, *112*, A10217, doi:10.1029/2007JA012495.

Lyons, L. R., T. Nishimura, X. Xing, A. Runov, V. Angelopoulos, E. F. Donovan, and T. Kikuchi (2012), Coupling of dipolarization front flow bursts to substorm expansion phase phenomena within the magnetosphere and ionosphere, *J. Geophys. Res.*, *117*, A02212, doi:10.1029/2011JA017265.

Mende, S. B., H. U. Frey, B. J. Morsony, and T. J. Immel (2003), Statistical behavior of proton and electron auroras during substorms, *J. Geophys. Res.*, *108*(A9), 1339, doi:10.1029/2002JA009751.

Mende, S. B., S. E. Harris, H. U. Frey, V. Angelopoulos, C. T. Russell, E. Donovan, B. Jackel, M. Greffen, and L. M. Peticolas (2008), The THEMIS array of ground-based observatories for the study of auroral substorms, *Space Sci. Rev.*, *141*, 357–387, doi:10.1007/s11214-008-9380-x.

Montbriand, L. E. (1971), The proton aurora and auroral substorm, in *The Radiating Atmosphere*, edited by B. M. McCormac, pp. 366–373, D. Reidel, Norwell, Mass.

Nakamura, R., et al. (2002), Motion of the dipolarization front during a flow burst event observed by Cluster, *Geophys. Res. Lett.*, *29*(20), 1942, doi:10.1029/2002GL015763.

Nakamura, R., et al. (2004), Flow shear near the boundary of the plasma sheet observed by Cluster and Geotail, *J. Geophys. Res.*, *109*, A05204, doi:10.1029/2003JA010174.

Ohtani, S., M. A. Shay, and T. Mukai (2004), Temporal structure of the fast convective flow in the plasma sheet: Comparison between observations and two-fluid simulations, *J. Geophys. Res.*, *109*, A03210, doi:10.1029/2003JA010002.

Raeder, J., D. Larson, W. H. Li, E. L. Kepko, and T. Fuller-Rowell (2008), OpenGGCM Simulations for the THEMIS mission, *Space Sci. Rev.*, *141*(1–4), 535–555, doi:10.1007/s11214-008-9421-5.

Runov, A., V. Angelopoulos, M. I. Sitnov, V. A. Sergeev, J. Bonnell, J. P. McFadden, D. Larson, K. H. Glassmeier, and U. Auster (2009), THEMIS observations of an earthward-propagating dipolarization front, *Geophys. Res. Lett.*, *36*, L14106, doi:10.1029/2009GL038980.

Runov, A., V. Angelopoulos, X.-Z. Zhou, X.-J. Zhang, S. Li, F. Plaschke, and J. Bonnell (2011a), A THEMIS multicase study of dipolarization fronts in the magnetotail plasma sheet, *J. Geophys. Res.*, *116*, A05216, doi:10.1029/2010JA016316.

Runov, A., et al. (2011b), Dipolarization fronts in the magnetotail plasma sheet, *Planet. Space Sci.*, *59*(7), 517–525, doi:10.1016/j.pss.2010.06.006.

Samson, J. C., L. R. Lyons, P. T. Newell, F. Creutzberg, and B. Xu (1992), Proton aurora and substorm intensifications, *Geophys. Res. Lett.*, *19*(21), 2167–2170.

Sergeev, V. A., and B. B. Gvozdevsky (1995), MT-index - a possible new index to characterize the magnetic configuration of magnetotail, *Ann. Geophys.*, *13*, 1093–1103, doi:10.1007/s00585-995-1093-9.

Sergeev, V. A., E. M. Sazhina, N. A. Tsyganenko, J. A. Lundblad, and F. Soraas (1983), Pitch-angle scattering of energetic protons in the magnetotail current sheet as the dominant source of their isotropic precipitation into the nightside ionosphere, *Planet. Space Sci.*, *31*(10), 1147–1155.

Sergeev, V. A., R. C. Elphic, F. S. Mozer, A. Saintmarc, and J. A. Sauvaud (1992), A 2-satellite study of nightside flux-transfer events in the plasma sheet, *Planet. Space Sci.*, *40*(11), 1551–1572.

Sergeev, V. A., V. Angelopoulos, J. T. Gosling, C. A. Cattell, and C. T. Russell (1996), Detection of localized, plasma-depleted flux tubes or bubbles in the midtail plasma sheet, *J. Geophys. Res.*, *101*(A5), 10,817–10,826.

Sergeev, V., V. Angelopoulos, S. Apatenkov, J. Bonnell, R. Ergun, R. Nakamura, J. McFadden, D. Larson, and A. Runov (2009), Kinetic structure of the sharp injection/dipolarization front in the flow-braking region, *Geophys. Res. Lett.*, *36*, L21105, doi:10.1029/2009GL040658.

Sitnov, M. I., M. Swisdak, and A. V. Divin (2009), Dipolarization fronts as a signature of transient reconnection in the magnetotail, *J. Geophys. Res.*, *114*, A04202, doi:10.1029/2008JA013980.

Slavin, J. A., R. P. Lepping, J. Gjerloev, D. H. Fairfield, M. Hesse, C. J. Owen, M. B. Moldwin, T. Nagai, A. Ieda, and T. Mukai (2003), Geotail observations of magnetic flux ropes in the plasma sheet, *J. Geophys. Res.*, *108*(A1), 1015, doi:10.1029/2002JA009557.

Takahashi, Y., and H. Fukunishi (2001), The dynamics of the proton aurora in auroral breakup events, *J. Geophys. Res.*, *106*(A1), 45–63.

Tang, C. L., V. Angelopoulos, A. Runov, C. T. Russell, H. Frey, K. H. Glassmeier, K. H. Fornacon, and Z. Y. Li (2010), Precursor activation and substorm expansion associated with observations of a dipolarization front by Thermal Emission Imaging System (THEMIS), *J. Geophys. Res.*, *115*, A07215, doi:10.1029/2009JA014879.

Wolf, R. A., Y. F. Wan, X. Xing, J. C. Zhang, and S. Sazykin (2009), Entropy and plasma sheet transport, *J. Geophys. Res.*, *114*, A00D05, doi:10.1029/2009JA014044.

Zesta, E., L. R. Lyons, and E. Donovan (2000), The auroral signature of Earthward flow bursts observed in the Magnetotail, *Geophys. Res. Lett.*, *27*(20), 3241–3244.

Zhou, X.-Z., V. Angelopoulos, V. A. Sergeev, and A. Runov (2010), Accelerated ions ahead of earthward propagating dipolarization fronts, *J. Geophys. Res.*, *115*, A00I03, doi:10.1029/2010JA015481.

Zhou, X.-Z., V. Angelopoulos, V. A. Sergeev, and A. Runov (2011), On the nature of precursor flows upstream of advancing dipolarization fronts, *J. Geophys. Res.*, *116*, A03222, doi:10.1029/2010JA016165.

Zhou, X.-Z., Y. S. Ge, V. Angelopoulos, A. Runov, J. Liang, X. Xing, J. Raeder, and Q.-G. Zong (2012), Dipolarization fronts and associated auroral activities: 2. Acceleration of ions and their subsequent behavior, *J. Geophys. Res.*, doi:10.1029/2012JA017677, in press.